Resolution-of-identity accelerated relativistic two- and four-component electron dynamics approach to chiroptical spectroscopies

Lukas Konecny,[1,2] Marius Kadek,[1] Stanislav Komorovsky,[3] Kenneth Ruud,[1] and Michal Repisky[1]

[1]*Hylleraas Centre for Quantum Molecular Sciences, Department of Chemistry, University of Tromsø—The Arctic University of Norway, Tromsø, Norway*
[2]*Department of Inorganic Chemistry, Faculty of Natural Sciences, Comenius University, Bratislava, Slovakia*
[3]*Institute of Inorganic Chemistry, Slovak Academy of Sciences, Bratislava, Slovakia*

We present an implementation and application of electron dynamics based on real-time time-dependent density functional theory (RT-TDDFT) and relativistic 2-component X2C and 4-component Dirac–Coulomb (4c) Hamiltonians to the calculation of electron circular dichroism and optical rotatory dispersion spectra. In addition, the resolution-of-identity approximation for the Coulomb term (RI-J) is introduced into RT-TDDFT and formulated entirely in terms of complex quaternion algebra. The proposed methodology was assessed on the dimethylchalcogenirane series, C_4H_8X (X = O, S, Se, Te, Po, Lv), and the spectra obtained by non-relativistic and relativistic methods start to disagree for Se and Te, while dramatic differences are observed for Po and Lv. The X2C approach, even in its simplest one-particle form, reproduces the reference 4c results surprisingly well across the entire series while offering an 8-fold speed-up of the simulations. An overall acceleration of RT-TDDFT by means of X2C and RI-J increases with system size and approaches a factor of almost 25 when compared to the full 4c treatment, without compromising the accuracy of the final spectra. These results suggest that one-particle X2C electron dynamics with RI-J acceleration is an attractive method for the calculation of chiroptical spectra in the valence region. *Published by AIP Publishing.*
https://doi.org/10.1063/1.5051032

I. INTRODUCTION

Chirality, i.e., non-superimposability of an object and its mirror image, is a ubiquitous phenomenon in chemistry and a prime example of the relationship between the molecular structure and properties. A pair of enantiomers, i.e., a chiral molecule and its mirror image, differs in its interaction with other chiral objects, including molecules or light. Notably, enantiomers possess different indices of refraction for left- and right-handed circularly polarized light.[1] The difference in the real (dispersive) part of the index of refraction is called circular birefringence and leads to optical rotation, i.e., rotation of the plane of polarization of linearly polarized light passing through an optically active medium, whereas the difference in the imaginary (absorptive) part of the index of refraction is called circular dichroism (CD) and leads to the generation of ellipticity in the linearly polarized light.[1–3] Optical rotation is measured either as the difference in refractive indices or as the angle of rotation of the linearly polarized light. Similarly, circular dichroism is measured either as the difference in extinction coefficients or as the induced ellipticity. The dependence of these properties on the frequency of light is called optical rotatory dispersion (ORD) or circular dichroism (CD) spectroscopy, respectively. CD spectra can be measured in the UV/Vis or X-ray regions as a result of transitions between electronic states—(X-ray) electron circular dichroism [(X)ECD].[4] In the IR region, the transitions occur between vibrational

states resulting in vibrational circular dichroism (VCD).[5] All these chiroptical spectroscopies play a crucial role in the identification of compounds or in the determination of absolute configurations, presenting a challenge for theory in terms of ensuring reliable computational results and an opportunity for theoretical chemistry to aid in the analysis of experimental data.[6–9]

The first-principles quantum-chemical determination of indices of refraction, or chiroptical spectra in general, requires the calculation of microscopic frequency-dependent molecular property tensors. In the context of time-dependent density functional theory (TDDFT), there are two main approaches that can be used. The first approach is based on perturbation theory and can proceed in two ways. One either calculates excitation energies and the corresponding transition moments followed by applying line shape functions to the calculated stick spectra.[10–12] Alternatively, one calculates the spectrum directly in the frequency domain using damped response theory.[13] Several applications to the calculations of chiropical properties have been reported and reviewed for TDDFT[14–21] as well as for post-Hartree–Fock methods such as coupled cluster (CC) theory.[22,23]

The second approach, which has gained increasing attention in recent years, considers the dynamics of molecules under the influence of external fields by propagating the electronic state directly in time, the so-called real-time (RT) TDDFT,[24–31] or similar post-Hartree–Fock dynamical

approaches.[32–37] Frequency-dependent molecular properties are then recovered as Fourier transforms of time-dependent properties recorded in the course of the simulations. Compared to perturbation theory-based approaches, real-time methods allow the description of molecules under strong external fields or external fields with complicated time dependence. Moreover, they can access spectra in various regions from a single run and do not require the evaluation of response kernels. On the other hand, long time propagations present a challenge in terms of computational cost, prompting the development of various acceleration techniques such as the time-dependent incremental Fock build method,[38] the non-recursive Chebyshev expansion,[39] the Padé approximants,[40] or the resolution-of-identity (RI) technique presented in this paper. Pioneering applications of RT-TDDFT to CD spectra have already been presented at the non-relativistic (1c) level of theory utilizing both real-space grids[41,42] and Gaussian orbitals.[43] For more information on real-time methodologies, the reader is referred to a recent review by Goings, Lestrange, and Li.[44]

In order to correctly describe molecules containing atoms from across the whole periodic table, one needs to take relativistic effects into account.[45] A typical approach in relativistic quantum chemistry is to combine the 4-component (4c) one-electron Dirac operator with a non-relativistic Coulomb interaction between the electrons into the 4c Dirac–Coulomb (DC) Hamiltonian. This currently represents the "gold standard" in relativistic quantum chemistry and can be used to benchmark more cost-effective approximate methods. One rung below the 4c Hamiltonians are the 2-component (2c) Hamiltonians, some of the popular and variationally stable ones being the second-order Douglas–Kroll–Hess (DKH2) Hamiltonian,[46–48] the zeroth-order regular approximation (ZORA) Hamiltonian,[49,50] the normalized elimination of small component (NESC) Hamiltonian,[51,52] and the closely related "exact" 2-component (X2C) Hamiltonian.[53–57] The X2C Hamiltonian, in particular, has seen growing interest in the relativistic quantum chemistry community in recent years,[58,59] as it allows for a reduction of the original 4c problem to 2c form at the expense of simple algebraic operations, thus yielding significant acceleration and still preserving most of the crucial relativistic contributions. The first implementation of 4c RT-TDDFT has been presented by Repisky *et al.*[60] followed by its application to X-ray absorption near-edge structure (XANES) spectra.[61] Later, it has been shown that the X2C transformation can be applied in the time-dependent context as well, provided the external field has a small amplitude or frequency.[62,63]

In this paper, we present an implementation of 4c- and X2C-based relativistic electron dynamics and its application to the chiroptical spectra of the benchmark dimethylchalcogenirane series, C_4H_8X (X = O, S, Se, Te, Po, Lv). We begin by defining the central chiroptical property tensor, then continue with the description of the relativistic density matrix propagation, and further formulate the RI approximation within RT-TDDFT. The paper ends with a discussion of the results, with an emphasis on relativistic effects and the accuracy and performance of the X2C method in combination with the RI acceleration.

II. THEORY

A. Chiroptical properties

The central microscopic molecular property that can be directly related to ORD and ECD is the electric dipole–magnetic dipole (Rosenfeld) tensor $\boldsymbol{\beta}$.[2,64] In the sum-over-states formalism, the ij Cartesian component of this tensor reads (in atomic units)

$$\beta_{ij}(\omega) = -2 \sum_{p \neq q} \frac{\Im\left(\langle p|\mu_i|q\rangle\langle q|m_j|p\rangle\right)}{\Omega_{qp}^2 - \omega^2}, \tag{1}$$

where p and q are the many-particle stationary states, $\Omega_{qp} = E_q - E_p$ is the energy/frequency difference, $\Im()$ refers to the imaginary part, $\boldsymbol{m}$ is the magnetic dipole, and $\boldsymbol{\mu}$ is the electric dipole moment operator, respectively. The Rosenfeld tensor connects the induced electric dipole moment to the time derivative of a magnetic field ($\boldsymbol{B}$) as well as the induced magnetic moment to the time derivative of an electric field ($\boldsymbol{E}$),[1]

$$\mu_i^{\mathrm{ind}}(\omega) = \beta_{ij}(\omega)\dot{B}_j(\omega) + \cdots, \tag{2}$$

$$m_i^{\mathrm{ind}}(\omega) = -\beta_{ji}(\omega)\dot{E}_j(\omega) + \cdots. \tag{3}$$

The ellipses stand for higher-order terms in electric and magnetic fields that can be neglected for isotropic samples and the weak-field regime, as considered in this study. In Sec. II B, we outline how to obtain the Rosenfeld tensor from electron dynamics simulations using Eq. (3).

B. Relativistic electron dynamics for chiroptical properties

The dynamics of electrons in the presence of a time-dependent external field is described by the Liouville–von Neumann equation,[65] which for Kohn-Sham RT-TDDFT[66] in an orthonormal basis takes the form

$$i\frac{\partial \mathbf{D}(t)}{\partial t} = [\mathbf{F}(t), \mathbf{D}(t)]. \tag{4}$$

In Eq. (4), $\mathbf{D}(t)$ is the one-electron reduced density matrix and $\mathbf{F}(t)$ is the Fock matrix constructed from $\mathbf{D}(t)$. Equation (4) is, therefore, non-linear and requires sophisticated propagation techniques.[60,67–74] Our implementation utilizes the Magnus expansion truncated to first order combined with an extrapolation–interpolation scheme.[60] The Fock matrix $\mathbf{F}(t)$ in Eq. (4) can be expressed as

$$\mathbf{F}(t) = \mathbf{h} + \mathbf{V}^{\mathrm{XC}}[\rho(t)] + \mathbf{G}[\mathbf{D}(t)] + \mathbf{V}^{\mathrm{ext}}(t), \tag{5}$$

where $\mathbf{h}$ is the one-electron term, $\mathbf{V}^{\mathrm{XC}}$ is the exchange–correlation potential matrix, and $\mathbf{G}$ is the two-electron term containing the Coulomb interaction $\mathbf{J}$ and, in the case of hybrid functionals, also the exchange interaction $\mathbf{K}$. $\mathbf{V}^{\mathrm{ext}}(t)$ is the time-dependent external field matrix that governs the time evolution of the system.

In 4c DC relativistic electron dynamics, the one-electron term is the matrix representation of the 4c one-electron Dirac Hamiltonian consisting of the kinetic contribution and the electron-nuclear Coulomb contribution, respectively. The two-electron term is constructed by assuming an instantaneous, non-relativistic Coulomb interaction between electrons. Similarly, the DFT exchange–correlation potential is expressed in its standard non-relativistic and adiabatic form, utilizing in

the current implementation a non-collinear formalism based on the spin magnetization vector,[75] as described in detail in Ref. 76.

The X2C Fock matrix is constructed by a block diagonalization of the original 4c Fock matrix and discarding the block with the negative-energy eigenspectrum. In an ideal case, such a procedure would require the X2C block-diagonalization of two-electron terms in each time step which leads to a method even more expensive than the full 4c treatment. Therefore, in practice, approximate solutions are sought after, both in the static[77–81] and dynamic (time-dependent) case.[62,63] In our present implementation, we apply the one-electron X2C approximation that only considers the block-diagonalization of the one-electron term, i.e.,

$$\mathbf{h}^{4c} \rightarrow \mathbf{h}^{X4C} \equiv \mathbf{U}^{\dagger}\mathbf{h}^{4c}\mathbf{U} = \begin{pmatrix} \mathbf{h}_{+}^{X4C} & 0 \\ 0 & \mathbf{h}_{-}^{X4C} \end{pmatrix} \rightarrow \mathbf{h}^{X2C} \equiv \mathbf{h}_{+}^{X4C}, \quad (6)$$

while adding the untransformed two-electron large–large block. The decoupling matrix $\mathbf{U}$ is built in a static case from eigenvectors of $\mathbf{h}^{4c}$ by solving algebraic equations.[55–57] In the dynamical regime, the decoupling matrix is in general time dependent; however, we neglect this time dependence by invoking an adiabatic approximation valid under conditions discussed in our previous work.[62] The detailed derivation of the X2C variant of the Liouville–von Neumann equation, as well as the decoupling procedure in the time regime, can be found in earlier work by Konecny *et al.*[62] and Goings *et al.*[63]

To calculate ECD and ORD spectra, the external perturbation potential in Eq. (5) takes the form of an electric pulse described within the dipole approximation as $\mathbf{V}^{ext}(t) = -\mathbf{P} \cdot \mathbf{E}(t)$, where $\mathbf{P}$ is the matrix representation of the electric dipole moment operator and $\mathbf{E}(t) = \boldsymbol{\kappa}\delta(t - t_0)$ is the external electric field with the vector amplitude $\boldsymbol{\kappa}$ and δ-functional time dependence. The ground-state self-consistent field (SCF) density matrix $\mathbf{D}_0$ is perturbed by this pulse, $\mathbf{D}(t_0) = \exp[-i\mathbf{P}]\mathbf{D}_0 \exp[i\mathbf{P}]$,[60] and evolved from an initial time t_0 in a series of discrete time steps of length Δt. In each time step t_j, the induced magnetic dipole moment is calculated from a trace of the magnetic dipole moment matrix and the time-dependent density matrix

$$\boldsymbol{m}^{ind}(t_j) = \text{Tr}[\mathbf{M}\mathbf{D}(t_j)] - \boldsymbol{m}^{static}, \quad (7)$$

where the static magnetic moment is calculated as $\boldsymbol{m}^{static} = \text{Tr}[\mathbf{M}\mathbf{D}_0]$. The recorded magnetic dipole moments are subsequently transformed to the frequency domain by means of a discrete Fourier transformation, while introducing an artificial damping factor γ to ensure finite width of the spectral lines,

$$\boldsymbol{m}^{ind}(\omega_k) = \sum_{j=0}^{n-1} \Delta t\, \boldsymbol{m}^{ind}(t_j)e^{-\gamma\,t_j}\exp\left\{2\pi i\frac{jk}{n}\right\}. \quad (8)$$

Here, $k = 0, 1, \ldots, n - 1$, where n is the number of time steps and $\omega_k = 2\pi k/\Delta t$ is the kth frequency point.

The frequency-dependent induced magnetic moment in Eq. (8) can be related to the expansion in Eq. (3) as

$$m_i^{ind}(\omega) = i\beta_{ji}(\omega)\kappa_j, \quad (9)$$

provided that higher order terms have been neglected in Eq. (3) and a δ-type impulse electric field was assumed as discussed in

the previous paragraph. The final expression for the Rosenfeld tensor thus reads

$$\beta_{ji}(\omega) = -i\frac{m_i^{ind}(\omega)}{\kappa_j}. \quad (10)$$

The ORD spectral function is then proportional to the real part of $\beta_{ji}(\omega)$ (or the imaginary part of $m_i^{ind}(\omega)$), and the ECD spectral function is proportional to the imaginary part of $\beta_{ji}(\omega)$ (or the real part of $m_i^{ind}(\omega)$).

Note that the procedure outlined above does not simulate the experimental ECD process directly but rather takes advantage of the fact that the Rosenfeld tensor that defines the lowest-order chiroptical properties also appears in other formulas, such as Eq. (3). Time-dependent magnetization induced by the electric component of the external radiation field described by Eq. (3) is more suitable for RT-TDSCF treatment.

A finite-basis representation of the magnetic dipole moment operator, denoted as $\mathbf{M}$ in Eq. (7), has the following forms in non-relativistic (1c) and 4c theories (in Hartree atomic units):

$$\boldsymbol{m}^{1c} = -\frac{1}{2c}\boldsymbol{r}_g \times \boldsymbol{p}, \quad (11)$$

$$\boldsymbol{m}^{4c} = -\frac{1}{2}\boldsymbol{r}_g \times \boldsymbol{\alpha}. \quad (12)$$

Here $\boldsymbol{\alpha}$ is the vector composed of Dirac's α matrices, $\boldsymbol{p}$ is the non-relativistic momentum operator, and $\boldsymbol{r}_g = \boldsymbol{r} - \boldsymbol{R}_g$ is the electron position operator relative to a fixed gauge, $\boldsymbol{R}_g$. All calculations presented in this paper assume the gauge placed in the centre of mass of the molecule. Although the present methodology is gauge dependent, this dependence is well established for ECD and ORD both at the non-relativistic and relativistic levels of theory,[10,17] and we have not explored this further here. In 4c theory, the operators are represented in a restricted kinetic balance (RKB) basis $\mathbf{X}^{4c}$, where the individual large (L) and small (S) component basis elements are defined as

$$\mathbf{X}_{\mu}^{4c} = \begin{pmatrix} \mathbf{X}_{\mu}^{L} & 0 \\ 0 & \mathbf{X}_{\mu}^{S} \end{pmatrix} = \begin{pmatrix} \boldsymbol{\sigma}_0 & 0 \\ 0 & (2c)^{-1}(\boldsymbol{\sigma}\cdot\boldsymbol{p}) \end{pmatrix}\chi_{\mu}(\boldsymbol{r}). \quad (13)$$

Here, $\boldsymbol{\sigma}_0$ is a 2×2 unit matrix, $\boldsymbol{\sigma}$ is the vector composed of Pauli matrices, and the functions $\chi_{\mu}(\boldsymbol{r})$ are elements of a real scalar basis set, in our implementation chosen to be Gaussian-type orbitals (GTOs). The elements of the 4c magnetic dipole moment matrix in the RKB basis are

$$\mathbf{M}_{\mu\nu}^{4c}$$
$$= -\frac{1}{4c}\begin{pmatrix} 0 & \langle\chi_{\mu}|(\boldsymbol{r}_g \times \boldsymbol{\sigma})(\boldsymbol{\sigma}\cdot\boldsymbol{p})|\chi_{\nu}\rangle \\ \langle\chi_{\mu}|(\boldsymbol{\sigma}\cdot\boldsymbol{p})(\boldsymbol{r}_g \times \boldsymbol{\sigma})|\chi_{\nu}\rangle & 0 \end{pmatrix}. \quad (14)$$

In X2C theory, the magnetic dipole matrix is given by a picture-change transformation of the original 4c dipole moment matrix using the aforementioned decoupling matrix $\mathbf{U}$ and leaving only its upper diagonal block, i.e.,

$$\mathbf{M}^{X2C} = \left[\mathbf{U}^{\dagger}\mathbf{M}^{4c}\mathbf{U}\right]_{+}, \quad (15)$$

which resembles the decoupling procedure for $\mathbf{h}^{4c}$ outlined in Eq. (6).

C. Resolution-of-identity for the Coulomb problem in RT-TDDFT

In the relativistic two- and four-component molecular electronic structure calculations, the Coulomb term in the Fock matrix,

$$\mathbf{J}_{\mu\nu}(t) = \sum_{\kappa\lambda}[\mathbf{\Omega}_{\mu\nu}|\text{Tr}(\mathbf{\Omega}_{\kappa\lambda}\mathbf{D}_{\lambda\kappa}(t))], \quad (16)$$

requires the evaluation of four-centre electron repulsion integrals (ERIs)

$$[\mathbf{\Omega}_{\mu\nu}|\mathbf{\Omega}_{\kappa\lambda}] \equiv \int \mathbf{X}_\mu^\dagger(\boldsymbol{r}_1)\mathbf{X}_\nu(\boldsymbol{r}_1)\frac{1}{r_{12}}\mathbf{X}_\kappa^\dagger(\boldsymbol{r}_2)\mathbf{X}_\lambda(\boldsymbol{r}_2)d\boldsymbol{r}_1 d\boldsymbol{r}_2, \quad (17)$$

where $\mathbf{X}_\mu$ refers to a multicomponent basis which, in accordance with Eq. (13), can be either $\mathbf{X}_\mu = \mathbf{X}_\mu^L$ for 2c theory or $\mathbf{X}_\mu = \mathbf{X}_\mu^{4c}$ for 4c theory. Due to the multicomponent nature, all elements associated with the basis, density matrix, or Coulomb matrix have an internal 2×2 or 4×4 structure, a fact that is indicated by bold symbols in our notation. Likewise, Tr() in Eq. (16) denotes the matrix trace over the multiple components.

To accelerate the evaluation of $\mathbf{J}$ by means of the resolution-of-identity, the electron repulsion integrals in Eq. (16) are approximated in the sense of a Dunlap's robust fit[82] by $\widetilde{[\mathbf{\Omega}_{\mu\nu}|\mathbf{\Omega}_{\kappa\lambda}]}$ such that the residual Coulomb-repulsion integral,

$$[\Delta\mathbf{\Omega}_{\mu\nu}|\Delta\mathbf{\Omega}_{\kappa\lambda}] = [\mathbf{\Omega}_{\mu\nu}|\mathbf{\Omega}_{\kappa\lambda}] - \widetilde{[\mathbf{\Omega}_{\mu\nu}|\mathbf{\Omega}_{\kappa\lambda}]}, \quad (18)$$

is bilinear in errors $\Delta\mathbf{\Omega}_{\mu\nu}$ and $\Delta\mathbf{\Omega}_{\kappa\lambda}$. It is customary to approximate the pairs of basis functions $|\mathbf{\Omega}_{\mu\nu}]$ as a superposition of real, scalar, atom-centered auxiliary basis functions $|\alpha]$; then,

$$|\Delta\mathbf{\Omega}_{\mu\nu}] = |\mathbf{\Omega}_{\mu\nu}] - \sum_\alpha \mathbf{c}_\alpha^{\mu\nu}|\alpha]. \quad (19)$$

The individual expansion coefficients $\mathbf{c}_\alpha^{\mu\nu}$ are then obtained by minimizing the residual Coulomb-repulsion integral with respect to $\mathbf{c}_\alpha^{\mu\nu}$. This leads to a set of linear equations

$$\sum_\beta [\alpha|\beta]\mathbf{c}_\beta^{\mu\nu} = [\alpha|\mathbf{\Omega}_{\mu\nu}], \quad (20)$$

whose solution when inserted into the expression for $\mathbf{J}$ with approximate integrals gives

$$\mathbf{J}_{\mu\nu}(t) \approx \sum_{\kappa\lambda}\sum_{\alpha\beta}[\mathbf{\Omega}_{\mu\nu}|\alpha][\alpha|\beta]^{-1}[\beta|\text{Tr}(\mathbf{\Omega}_{\kappa\lambda}\mathbf{D}_{\lambda\kappa}(t))]. \quad (21)$$

The original problem involving the evaluation of four-centre integrals is thus factorized into the product of two- and three-centre integrals, and the procedure is customarily denoted as the resolution-of-identity approximation for the Coulomb term (RI-J). The RI-J technique is widely used in non-relativistic molecular electronic structure calculations as it is known to affect the ground-state molecular energy by only 0.1 mhartree per atom, provided pre-optimized auxiliary sets are employed.[83] The approach has recently been extended also to the relativistic 4c domain.[84,85] However, it is not known if the RI-J approach is numerically stable for RT-TDDFT covering large time-propagation ranges.

In our implementation of RI-J within RT-TDDFT, the Coulomb term in Eq. (21) is calculated at every time point t_j in three steps: (a) 3-center ERIs are evaluated and contracted on-the-fly with the time-dependent density matrix, $\sum_{\kappa\lambda}[\alpha|\text{Tr}(\mathbf{\Omega}_{\kappa\lambda}\mathbf{D}_{\lambda\kappa}(t_j))] \equiv d_\alpha(t_j)$; (b) the linear set of equations derived from Eq. (20), $\sum_\beta[\alpha|\beta]c_\beta(t_j) = d_\alpha(t_j)$, is solved by means of a Cholesky decomposition; (c) 3-center ERIs are evaluated once again and contracted on-the-fly with the scalar expansion coefficients, $\sum_\beta[\mathbf{\Omega}_{\mu\nu}|\beta]c_\beta(t_j)$. The most time-consuming part of the algorithm is the first step, as its floating point operations (FLOPs) increase in the relativistic regime due to the multi-component character of the density matrix and basis elements as compared to the non-relativistic RT-TDDFT. However, the FLOPs can be greatly reduced in this case by reformulating the problem into the complex quaternion algebra, $\mathbb{H}_\mathbb{C}$, also known as biquaternion algebra. For example, every complex 2c density matrix $\mathbf{D}(t) \in \mathbb{C}^{2N\times 2N}$, which is Hermitian and does not impose any time-reversal symmetric structure

$$\mathbf{D}(t) = \begin{pmatrix} \mathbf{D_{11}} & \mathbf{D_{12}} \\ \mathbf{D_{21}} & \mathbf{D_{22}} \end{pmatrix}, \quad \mathbf{D_{11}, D_{12}, D_{21}, D_{22}} \in \mathbb{C}^{N\times N}, \quad (22)$$

can be mapped onto the matrix of complex quaternions, $^Q\mathbf{D}(t) \in \mathbb{H}_\mathbb{C}^{N\times N}$,

$$\mathbf{D} \to {}^Q\mathbf{D} = ({}^0\mathbf{D}+i\,{}^4\mathbf{D})+({}^1\mathbf{D}+i\,{}^5\mathbf{D})\breve{i}+({}^2\mathbf{D}+i\,{}^6\mathbf{D})\breve{j}+({}^3\mathbf{D}+i\,{}^7\mathbf{D})\breve{k}, \quad (23)$$

where i stands for the imaginary unit and $1, \breve{i}, \breve{j}$ and $\breve{k}$ denote the basis elements of $\mathbb{H}_\mathbb{C}$ which obey the identities

$$\breve{i}^2 = \breve{j}^2 = \breve{k}^2 = \breve{i}\breve{j}\breve{k} = -1. \quad (24)$$

Note that these relations also determine all the possible products of $\breve{i}, \breve{j},$ and $\breve{k}$. The complex quaternion constituents $^{0-7}\mathbf{D} \in \mathbb{R}^{N\times N}$ are given by

$$\begin{aligned} {}^0\mathbf{D} &= \mathfrak{R}(\mathbf{D_{11}} + \mathbf{D_{22}^*})/2, & {}^4\mathbf{D} &= \mathfrak{I}(\mathbf{D_{11}} - \mathbf{D_{22}^*})/2, \\ {}^1\mathbf{D} &= \mathfrak{I}(\mathbf{D_{11}} + \mathbf{D_{22}^*})/2, & {}^5\mathbf{D} &= -\mathfrak{R}(\mathbf{D_{11}} - \mathbf{D_{22}^*})/2, \\ {}^2\mathbf{D} &= \mathfrak{R}(\mathbf{D_{12}} - \mathbf{D_{21}^*})/2, & {}^6\mathbf{D} &= \mathfrak{I}(\mathbf{D_{12}} + \mathbf{D_{21}^*})/2, \\ {}^3\mathbf{D} &= \mathfrak{I}(\mathbf{D_{12}} - \mathbf{D_{21}^*})/2, & {}^7\mathbf{D} &= -\mathfrak{R}(\mathbf{D_{12}} + \mathbf{D_{21}^*})/2 \end{aligned} \quad (25)$$

and have the following matrix properties:

$$^k\mathbf{D} = {}^k\mathbf{D}^T, \quad {}^l\mathbf{D} = -{}^l\mathbf{D}^T, \quad k \in 0, 5, 6, 7, \quad l \in 1, 2, 3, 4. \quad (26)$$

Considering the properties in Eq. (26) as well as the fact that the matrix of 2c overlap distributions, $\mathbf{\Omega}(\boldsymbol{r}) \equiv (\mathbf{X}^L)^\dagger \mathbf{X}^L \in \mathbb{C}^{2N\times 2N}(\mathbb{R}^3)$, has in its complex quaternion representation only one non-zero component, i.e.,

$$\mathbf{\Omega} \to {}^Q\mathbf{\Omega} = {}^0\mathbf{\Omega}, \quad (27)$$

the entire contribution to $\sum_{\kappa\lambda}[\alpha|\text{Tr}(\mathbf{\Omega}_{\kappa\lambda}\mathbf{D}_{\lambda\kappa}(t_j))]$ arises only from a single component of the complex quaternion trace

$$2\sum_{\kappa\lambda}[\alpha|{}^0\Omega_{\kappa\lambda}]{}^0 D_{\lambda\kappa}(t_j). \quad (28)$$

Note that the proposed quaternion-based 2c RI-J procedure gives rise to exactly the same number of real arithmetic operations as RI-J in the 1c unrestricted SCF.

In the 4c case, the formulation and evaluation of the Coulomb term in terms of complex quaternion algebra are slightly more elaborate. First, it involves a reordering of basis set components discussed by Saue *et al.*,[86] followed by a mapping of the 4c time-dependent density matrix $\mathbf{D}(t) \in \mathbb{C}^{4N\times 4N}$ and of the 4c overlap distribution matrix

$\mathbf{\Omega}(\mathbf{r}) \equiv \left(\mathbf{X}^{4c}\right)^{\dagger} \mathbf{X}^{4c} \in \mathbb{C}^{4N \times 4N}(\mathbb{R}^3)$ into complex quaternions in the sense of Eq. (23), the latter being

$$\mathbf{\Omega}(\mathbf{r}) \rightarrow{}^Q\mathbf{\Omega}(\mathbf{r}) = {}^0\mathbf{\Omega} + {}^1\mathbf{\Omega}\check{i} + {}^2\mathbf{\Omega}\check{j} + {}^3\mathbf{\Omega}\check{k} \in \mathbb{H}_{\mathbb{C}}^{2N \times 2N}(\mathbb{R}^3). \quad (29)$$

Here, the imaginary quaternion constituents ${}^{4-7}\mathbf{\Omega}(\mathbf{r}) \in \mathbb{R}^{2N \times 2N}(\mathbb{R}^3)$ are zero, whereas the real constituents ${}^{0-3}\mathbf{\Omega}(\mathbf{r}) \in \mathbb{R}^{2N \times 2N}(\mathbb{R}^3)$ are non-zero and for $k, l \in x, y, z$, read

$$
\begin{aligned}
{}^0\mathbf{\Omega}_{\mu\nu} &= \begin{pmatrix} \chi_\mu \chi_\nu & 0 \\ 0 & (\nabla_k \chi_\mu)(\nabla_k \chi_\nu) \end{pmatrix}, \\
{}^1\mathbf{\Omega}_{\mu\nu} &= \begin{pmatrix} 0 & 0 \\ 0 & \varepsilon_{zkl}(\nabla_k \chi_\mu)(\nabla_l \chi_\nu) \end{pmatrix}, \\
{}^2\mathbf{\Omega}_{\mu\nu} &= \begin{pmatrix} 0 & 0 \\ 0 & \varepsilon_{ykl}(\nabla_k \chi_\mu)(\nabla_l \chi_\nu) \end{pmatrix}, \\
{}^3\mathbf{\Omega}_{\mu\nu} &= \begin{pmatrix} 0 & 0 \\ 0 & \varepsilon_{xkl}(\nabla_k \chi_\mu)(\nabla_l \chi_\nu) \end{pmatrix},
\end{aligned}
\quad (30)
$$

where ε is the Levi-Civita symbol. In the formulation presented, the evaluation of the 4c trace in expression $\sum_{\kappa\lambda}[\alpha|\text{Tr}(\mathbf{\Omega}_{\kappa\lambda}\mathbf{D}_{\lambda\kappa}(t_j))]$ reduces only to the following four terms:

$$2 \sum_{\kappa\lambda} \sum_{k=0}^{3} [\alpha|{}^k\Omega_{\kappa\lambda}]{}^k D_{\lambda\kappa}(t_j), \quad (31)$$

which require just real (time-reversal symmetric) constituents of the complex quaternion density matrix. Note that the use of quaternion algebra for reducing the computation burden of relativistic 4c calculations has already been advocated by several authors, with a primary focus either on the diagonalization[86–88] or on the relativistic point group symmetry.[89] All these approaches, however, are limited to Kramers-restricted (closed-shell) molecular cases and thus involve only the *real* quaternions. Instead, the present approach based on a generalized concept of *complex* quaternions focuses mainly on reducing arithmetic operations associated with the Fock matrix construction. In addition, the use of complex quaternions allows to elegantly address the Kramers-unrestricted (open-shell) regime, which is indispensable in the real-time TDDFT calculations.

III. COMPUTATIONAL DETAILS

Geometries for lighter dimethylchalcogeniranes C_4H_8X with X = O, S were taken from other study,[19] while for X = Se, Te, Po, Lv, the geometries were optimized using the Amsterdam Density Functional (ADF) program suite[90–92] with the scalar ZORA Hamiltonian (Se, Te) and with the spin-orbit ZORA Hamiltonian (Po, Lv), employing the Perdew-Burke-Ernzerhof (PBE) functional[93–95] and the ZORA/TZ2P Slater-type orbital (STO) basis set.[96] All geometries can be found in the supplementary material.

All property calculations were performed with a developer's version of the ReSpect program[97] using the PBE functional.[93–95] All-electron GTO basis sets were employed in their uncontracted form, namely, Dyall's augmented cVDZ basis[98–100] for Te, Po, and Lv and Dunning's augmented cc-pVDZ basis[101–103] for all other elements. The auxiliary basis sets for the RI-J procedure were generated by an adjusted even-tempered algorithm[104] and are available in the

supplementary material. The numerical integration of the exchange–correlation potential was done with an adaptive molecular grid of medium size (program default), employing a noncollinear approach within the Kramer's unrestricted formalism, as specified by Komorovsky *et al.*[76] In 2c and 4c calculations, atomic nuclei of finite size were approximated by the Gaussian charge distribution model.[105] For the evaluation of four-center two-electron repulsion integrals in the 4c theory, we employed an atom-pair approximation where all integrals over the atom-centered small-component basis functions X^S are discarded unless the bra and ket basis pairs share the same origin, i.e., $[X_A^S X_B^S | X_C^S X_D^S]\delta_{AB}\delta_{CD}.$. Here, δ is the Kronecker delta function over atomic centers A, B, C, and D.

The elements β_{ji} of the Rosenfeld tensor were calculated using Eq. (10) from three simulations where the molecules were perturbed by external electric fields in directions x, y, and z. The amplitude of the delta function perturbation was in each simulation $\kappa_i = 0.0001$ a.u., i $\in \{x, y, z\}$. The time evolution was carried out for 30 000 time steps of length 0.15 a.u. (0.0036 fs) which corresponds to a total simulation time of approximately 109 fs and frequency-domain resolution 0.0014 a.u. (0.038 eV). Convergence thresholds for the microiterations in the Magnus propagator were set to 10^{-6}. The transformation to the frequency domain was performed by the discreet Fourier transformation utility in the SciPy package.[106] The final spectra were broadened by a damping factor $\gamma = 0.004$ a.u. [see Eq. (8)].

IV. RESULTS AND DISCUSSION

We demonstrate the use of relativistic electron dynamics for the calculation of chiroptical properties of a series of dimethylchalcogeniranes C_4H_8X, where X = O, S, Se, Te, Po, Lv (see Fig. 1). Dimethyloxirane is a prototypical chiral molecule used as a benchmark system for chiroptical properties, whereas dimethylthiirane and other heavier analogs were selected to determine the effect of relativistic treatment on the spectra and to assess the performance of X2C and RI-J acceleration. As a spectral function, we plot the isotropic value of the Rosenfeld tensor

$$S(\omega) = \frac{1}{3} \sum_i \beta_{ii}(\omega). \quad (32)$$

We first investigate the performance of the RI-J technique in the context of time-dependent relativistic methods by calculating the ECD and ORD spectra of dimethyltelirane with and without the RI-J approximation. The final spectra obtained with the 4c Hamiltonian are reported in Fig. 2, whereas corresponding results for the X2C Hamiltonian, that resembles the reference 4c data, are available in the supplementary material (Fig. 1). Visual inspection of the lines in Fig. 2 shows perfect agreement between the pairs of 4c and RI-J 4c spectra

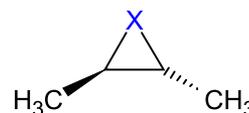FIG. 1. Structural formula of (2R, 3R)-2,3-dimethylchalcogenirane C_4H_8X (X = O, S, Se, Te, Po, Lv).
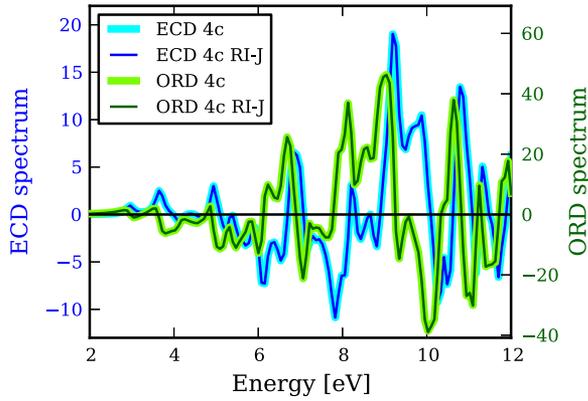
FIG. 2. The comparison of 4c ECD and ORD spectra (in atomic units) of the Te-based system calculated with and without the RI-J acceleration. The simulation proceeded for 15 000 time steps of length 0.15 a.u.

in the valence region. However, it is desirable to quantify this agreement. In time-independent RI-J calculations, it is customary to assess the RI-J by evaluating the energy difference per atom:[83] $\Delta E = |E^{exact} - E^{RI-J}|/N_{atom}$. Here, we extended this concept to the time domain by time-averaging of the energy error function ΔE,

$$\overline{\Delta E}(t_0, t_{max}) \equiv \frac{1}{t_{max} - t_0} \int_{t_0}^{t_{max}} \frac{|E^{exact}(t) - E^{RI-J}(t)|}{N_{atom}} dt, \quad (33a)$$

$$\approx \frac{1}{n_{steps}} \sum_{j=1}^{n_{steps}} \frac{|E^{exact}(t_j) - E^{RI-J}(t_j)|}{N_{atom}}. \quad (33b)$$

Equation (33a) thus defines the difference between the exact energy per atom and its RI-J approximant over a whole interval of propagation from t_0 to t_{max}. Since the propagation is performed in a series of discrete time steps, Eq. (33b) is used in practice. For the simulation that yields to the spectra on Fig. 2, $\overline{\Delta E}$(0 a.u., 2250 a.u.) is equal to $1.4 \cdot 10^{-6}$ a.u., which agrees with ΔE observed in the static case. A summary of $\overline{\Delta E}(t_0, t_{max})$ for the entire dimethylchalcogenirane series as obtained from the first 10 000 time steps is listed in Table I. In all cases, the time-averaged energy error remains sufficiently small and RI-J typically affects energies by only 10^{-6} a.u. per atom, regardless of the relativistic Hamiltonian used.

Since the main quantities of interest in RT-TDDFT property calculations are frequency-dependent spectral functions,

$\overline{\Delta E}(t_0, t_{max})$ may not be the most suitable quantity to measure the accuracy of RI-J. Therefore, we extended the concept of averaged energy error functions from the time domain to the frequency domain by introducing the following spectral-function error:

$$\overline{\Delta S}(\omega_0, \omega_{max}) \equiv \frac{1}{\omega_{max} - \omega_0} \int_{\omega_0}^{\omega_{max}} \frac{|S^{exact}(\omega) - S^{RI-J}(\omega)|}{N_{atom}} d\omega, \quad (34a)$$

$$\approx \frac{1}{n_{steps}} \sum_{j=1}^{n_{steps}} \frac{|S^{exact}(\omega_j) - S^{RI-J}(\omega_j)|}{N_{atom}}, \quad (34b)$$

where again, Eq. (34a) is the definition for an ideal continuous case, whereas Eq. (34b) is its discretized variant used in practice. The values of $\overline{\Delta S}(\omega_0, \omega_{max})$ for ECD and ORD spectra presented on Fig. 2 are $\overline{\Delta S}_{ECD}$(0 eV, 12 eV) = $1.3 \cdot 10^{-4}$ a.u. and $\overline{\Delta S}_{ORD}$(0 eV, 12 eV) = $4.1 \cdot 10^{-4}$ a.u., respectively. A summary of $\overline{\Delta S}(\omega_0, \omega_{max})$ for the entire dimethylchalcogenirane series as obtained from the first 10 000 time steps is listed in Table I.

Encouraged by these results, we applied the RI-J accelerated simulations to the remaining systems. Graphs in Fig. 3 show how ECD spectra obtained from non-relativistic and relativistic methods differ across the series. While there is practically no difference for O and S (depicted in the supplementary material), the differences become noticeable starting with Se and Te. For the Po- and Lv-substituted systems, the 1c results cannot be considered even as an approximation of the relativistic results. Particularly, for the Po system, the 1c spectra resemble the mirror image of the relativistic spectra in a region from approximately 4.5 to 7 eV meaning that an assignment of absolute configuration just from this spectral region would be wrong. The result for the Po system demonstrates the possibility of 1c and 4c spectra looking like mirror images, a phenomenon that can span over a larger spectral range for a different system making 1c calculations unsuitable for interpreting ECD measurements in molecules where relativistic effects are prominent. Moreover, Fig. 3 shows that the X2C approach reproduces the reference 4c results surprisingly well across the entire series with only minor differences for the heaviest elements. Similar conclusions can be drawn about the ORD spectra, as supported by the figures available in the supplementary material.

TABLE I. Assessment of the accuracy of the RI-J approach in the relativistic two-component (2c) and four-component (4c) RT-TDDFT calculations of the chiroptical ECD and ORD spectra of dimethylchalcogeniranes C_4H_8X (X = O, S, Se, Te, Po, Lv) using the energy error function of Eq. (33b), $\overline{\Delta E}(t_0, t_{max})$, and the spectral error functions of Eq. (34b), $\overline{\Delta S}_{ECD}(\omega_0, \omega_{max})$ and $\overline{\Delta S}_{ORD}(\omega_0, \omega_{max})$. All results are reported in atomic units and were obtained from the first 10 000 time steps of length 0.15 a.u. that corresponds to the total simulation time $t_{max} \simeq 36.3$ fs. The maximum spectral frequency ω_{max} was set to 0.45 a.u. $\simeq$ 12.2 eV.

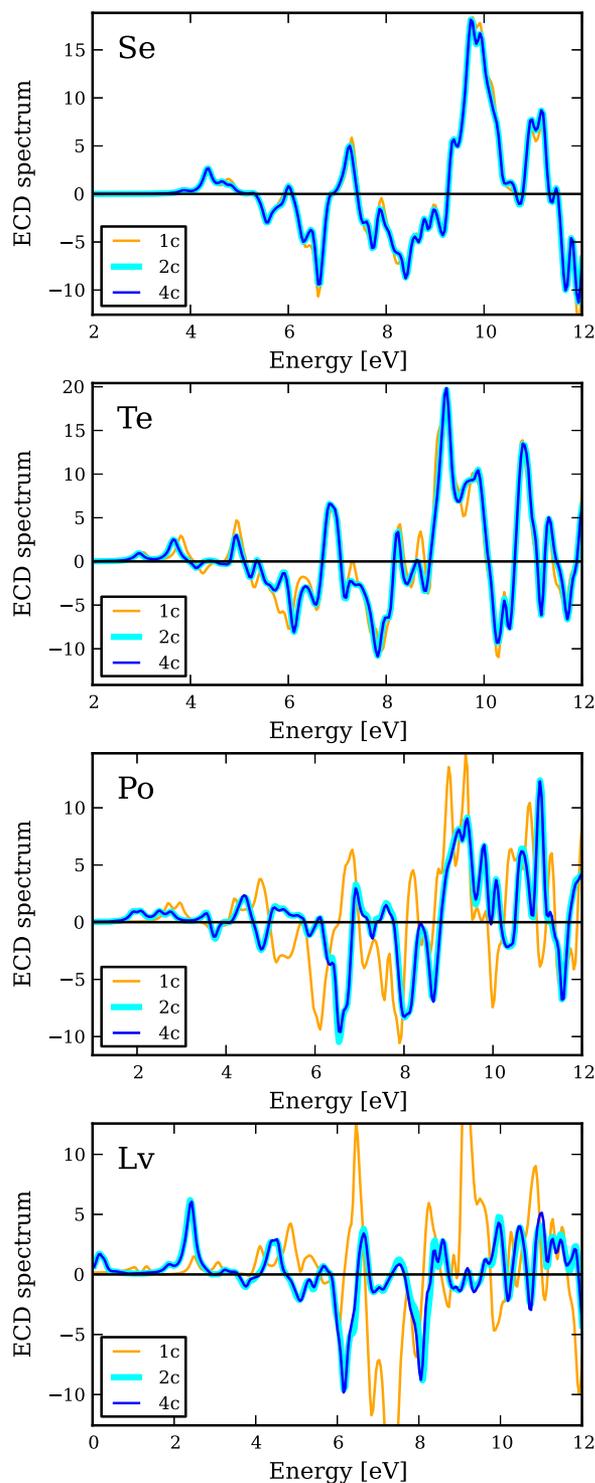| Heteroatom	$\overline{\Delta E}$(0 fs, 36.3 fs)		$\overline{\Delta S}_{ECD}$(0 eV, 12.2 eV)		$\overline{\Delta S}_{ORD}$(0 eV, 12.2 eV)	
	4c	2c	4c	2c	4c	2c
O	$2.7 \cdot 10^{-6}$	$2.7 \cdot 10^{-6}$	$2.4 \cdot 10^{-4}$	$6.7 \cdot 10^{-5}$	$1.9 \cdot 10^{-4}$	$6.7 \cdot 10^{-5}$
S	$2.6 \cdot 10^{-6}$	$3.9 \cdot 10^{-6}$	$2.7 \cdot 10^{-4}$	$1.2 \cdot 10^{-4}$	$3.0 \cdot 10^{-4}$	$1.1 \cdot 10^{-4}$
Se	$3.4 \cdot 10^{-6}$	$3.5 \cdot 10^{-6}$	$5.1 \cdot 10^{-4}$	$9.0 \cdot 10^{-5}$	$5.1 \cdot 10^{-4}$	$8.8 \cdot 10^{-5}$
Te	$1.4 \cdot 10^{-6}$	$1.6 \cdot 10^{-6}$	$1.3 \cdot 10^{-3}$	$9.7 \cdot 10^{-5}$	$1.5 \cdot 10^{-3}$	$9.7 \cdot 10^{-5}$
Po	$7.9 \cdot 10^{-8}$	$1.5 \cdot 10^{-6}$	$4.0 \cdot 10^{-3}$	$5.4 \cdot 10^{-3}$	$4.0 \cdot 10^{-3}$	$4.1 \cdot 10^{-3}$
Lv	$6.5 \cdot 10^{-8}$	$1.7 \cdot 10^{-6}$	$5.3 \cdot 10^{-3}$	$5.2 \cdot 10^{-5}$	$5.2 \cdot 10^{-3}$	$5.5 \cdot 10^{-5}$

FIG. 3. The comparison of 1c, 2c (X2C), and 4c (DC) ECD spectra (in atomic units) of dimethylchalcogeniranes computed using the PBE functional with RI-J acceleration. The corresponding spectra are labeled by the chemical symbol of the heteroatom. The ECD spectra of lighter analogs and all ORD spectra can be found in the supplementary material.

TABLE II. Wall-clock times per microiteration (in s) and achieved accelerations for the relativistic electron dynamics simulations with 4c and X2C Hamiltonians using exact four-centre integrals or the RI-J technique. The accelerations are reported in parentheses. The calculations were performed with OpenMP parallelization on a single node equipped with a dual-socket Intel Xeon processor (E5-2680v3, 2.5 GHz) with 12 CPU cores per socket.

	4c		X2C	
Heteroatom	Exact	RI-J[a]	Exact[b]	RI-J[c]
O	11.0	5.9 (1.9)	1.4 (7.7)	0.8 (1.9)
S	12.4	6.2 (2.0)	1.6 (7.6)	0.8 (2.0)
Se	15.7	7.1 (2.2)	2.1 (7.6)	1.0 (2.1)
Te	23.4	9.1 (2.6)	3.1 (7.6)	1.3 (2.3)
Po	42.7	11.6 (3.7)	4.9 (8.7)	1.8 (2.7)
Lv	50.6	12.7 (4.0)	5.7 (8.8)	2.2 (2.7)

[a]Acceleration calculated as the time ratio of exact vs. RI-J for 4c.
[b]Acceleration calculated as the time ratio of 4c vs. X2C for exact J.
[c]Acceleration calculated as the time ratio of exact vs. RI-J for X2C.

X2C Hamiltonian of C_4H_8Se to 4.0 for the 4c Hamiltonian of C_4H_8Lv. Note that these values do not reflect the actual acceleration associated with the evaluation of the Coulomb term but rather refer to the whole microiteration speed-up that also involves a diagonalization. Since the diagonalization step dominates in some cases, the overall effectiveness of RI-J may be reduced within RT-TDDFT when compared to the time-independent regime. However, a positive observation is that for both relativistic Hamiltonians, larger systems benefit more from RI-J. This trend is more pronounced for the 4c Hamiltonian, where the calculation of the two-electron contribution is by far the most time-consuming step. Moreover, orbital basis-function products over both the large and small component basis are fitted by an identical auxiliary basis set. The observed acceleration when going from 4c to X2C ranges from 7.6 to 8.8 and agrees with our previous findings.[62] The overall acceleration provided by the combination of the X2C and RI-J methodologies ranges from 14.3 to 23.5 for the systems studied when compared to the full 4c treatment, without compromising the accuracy of final spectra. These results suggest that one-particle X2C electron dynamics with RI-J acceleration is a viable and promising method for calculations of chiroptical spectra in the valence region.

V. CONCLUSIONS AND PERSPECTIVES

We have presented an implementation of relativistic Liouville–von Neumann electron dynamics based on 4c Dirac–Coulomb and 2c X2C Hamiltonians and its application to the prediction of chiroptical spectra via the analysis of time-dependent induced magnetic dipole moments. The implementation was further enhanced by the resolution-of-identity approximation for the Coulomb term (RI-J), a relativistic formulation of which has been presented for the first time in terms of complex quaternion algebra. The proposed methodology was assessed on the dimethylchalcogenirane series, C_4H_8X (X = O, S, Se, Te, Po, Lv), and it was observed that while the RI-J alone offers a speedup at least of a factor of two, the combination of the X2C Hamiltonian and RI-J can lead to almost 25-fold acceleration compared to the full 4c treatment. The RI-J acceleration is observed to be increasing with system size in

Finally, to assess the acceleration of RT-TDDFT achieved by the introduction of the RI-J technique, we report in Table II the average time per microiteration of the propagation solver. These values were obtained from the first 50 time steps (each time step required on average approximately 3 microiterations) and the achieved accelerations range from 2.1 for the

the studied series, and the trend is expected to hold making the methodology even more promising as one starts to consider larger molecules.

The calculation for the dimethylchalcogeniranes showed increasing importance of relativistic effects with increasing atomic number. Most notably, for the Po system, the 1c ECD spectrum was a mirror image of the relativistic spectrum in a certain frequency region, highlighting the necessity of a relativistic treatment when interpreting the spectra of molecules containing heavy elements. Furthermore, the X2C approach, even in its simplest one-particle form, reproduced the reference 4c results surprisingly well across the entire series. All these findings suggest that the RI-J-based relativistic electron dynamics, in particular, when combined with the X2C Hamiltonian, is a viable and promising tool for the calculation of chiroptical spectra in the valence region.

The methodology presented can be further extended by introducing the RI approximation for the exchange term (RI-K), allowing accelerated calculations also with hybrid DFT functionals. In addition, chiroptical spectroscopy in X-ray regions is another exciting area of research where relativistic corrections are expected to play a significant role and this line of investigation is currently pursued in our laboratory.

SUPPLEMENTARY MATERIAL

See supplementary material for molecular geometries, auxiliary basis sets, and additional ECD and ORD spectra.

ACKNOWLEDGMENTS

[1] L. D. Barron, *Molecular Light Scattering and Optical Activity* (Cambridge University Press, 2004).

[2] E. U. Condon, Rev. Mod. Phys. **9**, 432 (1937).

[3] A. E. Hansen and T. D. Bouman, Adv. Chem. Phys. **44**, 545 (1980).

[4] N. Berova, K. Nakanishi, and R. Woody, *Circular Dichroism: Principles and Applications* (John Wiley & Sons, 2000).

[5] P. J. Stephens, F. J. Devlin, and J. R. Cheeseman, *VCD Spectroscopy for Organic Chemists* (CRC Press, 2012).

[6] N. Berova, L. Di Bari, and G. Pescitelli, Chem. Soc. Rev. **36**, 914 (2007).

[7] G. Pescitelli, L. Di Bari, and N. Berova, Chem. Soc. Rev. **40**, 4603 (2011).

[8] H.-J. Zhu, *Organic Stereochemistry: Experimental and Computational Methods* (John Wiley & Sons, 2015).

[9] G. Pescitelli and T. Bruhn, Chirality **28**, 466 (2016).

[10] K. L. Bak, A. E. Hansen, K. Ruud, T. Helgaker, J. Olsen, and P. Jørgensen, Theor. Chim. Acta **90**, 441 (1995).

[11] S. Grimme, Chem. Phys. Lett. **339**, 380 (2001).

[12] J. Autschbach, T. Ziegler, S. J. van Gisbergen, and E. J. Baerends, J. Chem. Phys. **116**, 6930 (2002).

[13] P. Norman, K. Ruud, and T. Helgaker, J. Chem. Phys. **120**, 5027 (2004).

[14] P. Stephens, F. Devlin, J. Cheeseman, and M. Frisch, J. Phys. Chem. A **105**, 5356 (2001).

[15] J. Autschbach, S. Patchkovskii, T. Ziegler, S. J. van Gisbergen, and E. Jan Baerends, J. Chem. Phys. **117**, 581 (2002).

[16] J. Autschbach, F. E. Jorge, and T. Ziegler, Inorg. Chem. **42**, 2867 (2003).

[17] M. Pecul, K. Ruud, and T. Helgaker, Chem. Phys. Lett. **388**, 110 (2004).

[18] J. Autschbach, ChemPhysChem **12**, 3224 (2011).

[19] M. Srebro, N. Govind, W. A. De Jong, and J. Autschbach, J. Phys. Chem. A **115**, 10930 (2011).

[20] I. Warnke and F. Furche, Wiley Interdiscip. Rev. Comput. Mol. Sci. **2**, 150 (2012).

[21] M. Srebro-Hooper and J. Autschbach, Annu. Rev. Phys. Chem. **68**, 399 (2017).

[22] K. Ruud and T. Helgaker, Chem. Phys. Lett. **352**, 533 (2002).

[23] T. D. Crawford, Theor. Chem. Acc. **115**, 227 (2006).

[24] J. Theilhaber, Phys. Rev. B **46**, 12990 (1992).

[25] K. Yabana and G. Bertsch, Phys. Rev. B **54**, 4484 (1996).

[26] A. Tsolakidis, D. Sánchez-Portal, and R. Martin, Phys. Rev. B **66**, 235416 (2002).

[27] R. Baer and D. Neuhauser, J. Chem. Phys. **121**, 9803 (2004).

[28] C. M. Isborn and X. Li, J. Chem. Phys. **129**, 204107 (2008).

[29] K. Lopata and N. Govind, J. Chem. Theory Comput. **7**, 1344 (2011).

[30] K. J. Koh, T. S. Nguyen-Beck, and J. Parkhill, J. Chem. Theory Comput. **13**, 4173 (2017).

[31] I. Schelter and S. Kümmel, J. Chem. Theory Comput. **14**, 1910 (2018).

[32] T. Sato and K. L. Ishikawa, Phys. Rev. A **88**, 023402 (2013).

[33] P. Krause, T. Klamroth, and P. Saalfrank, J. Chem. Phys. **123**, 074105 (2005).

[34] D. Hochstuhl and M. Bonitz, Phys. Rev. A **86**, 053424 (2012).

[35] S. Bauch, L. K. Sørensen, and L. B. Madsen, Phys. Rev. A **90**, 062508 (2014).

[36] C. Huber and T. Klamroth, J. Chem. Phys. **134**, 054113 (2011).

[37] D. R. Nascimento and A. E. DePrince III, J. Chem. Theory Comput. **12**, 5834 (2016).

[38] W. Liang, C. T. Chapman, and X. Li, J. Chem. Phys. **134**, 184102 (2011).

[39] D. Williams-Young, J. J. Goings, and X. Li, J. Chem. Theory Comput. **12**, 5333 (2016).

[40] A. Bruner, D. LaMaster, and K. Lopata, J. Chem. Theory Comput. **12**, 3741 (2016).

[41] K. Yabana and G. Bertsch, Phys. Rev. A **60**, 1271 (1999).

[42] D. Varsano, L. A. Espinosa-Leal, X. Andrade, M. A. Marques, R. Di Felice, and A. Rubio, Phys. Chem. Chem. Phys. **11**, 4481 (2009).

[43] J. J. Goings and X. Li, J. Chem. Phys. **144**, 234102 (2016).

[44] J. J. Goings, P. J. Lestrange, and X. Li, Wiley Interdiscip. Rev.: Comput. Mol. Sci. **8**(1), e1341 (2018).

[45] P. Pyykkö, Annu. Rev. Phys. Chem. **63**, 45 (2012).

[46] M. Douglas and N. M. Kroll, Ann. Phys. **82**, 89 (1974).

[47] B. A. Hess, Phys. Rev. A **32**, 756 (1985).

[48] A. Wolf, M. Reiher, and B. A. Hess, J. Chem. Phys. **117**, 9215 (2002).

[49] C. Chang, M. Pelissier, and P. Durand, Phys. Scr. **34**, 394 (1986).

[50] E. V. Lenthe, E. J. Baerends, and J. G. Snijders, J. Chem. Phys. **99**, 4597 (1993).

[51] K. G. Dyall, J. Chem. Phys. **106**, 9618 (1997).

[52] D. Cremer, W. Zou, and M. Filatov, Wiley Interdiscip. Rev.: Comput. Mol. Sci. **4**, 436 (2014).

[53] J. L. Heully, I. Lindgren, E. Lindroth, S. Lundqvist, and A. M. Martensson-Pendrill, J. Phys. B: At., Mol. Phys. **19**, 2799 (1986).

[54] H. J. A. Jensen, "Douglas–Kroll the easy way," in The Conference Talk, REHE 2005, Mülheim, Germany.

[55] W. Kutzelnigg and W. Liu, J. Chem. Phys. **123**, 241102 (2005).

[56] W. Liu and W. Kutzelnigg, J. Chem. Phys. **126**, 114107 (2007).

[57] M. Iliaš and T. Saue, J. Chem. Phys. **126**, 064102 (2007).

[58] T. Saue, ChemPhysChem **12**, 3077 (2011).

[59] W. Liu, Phys. Rep. **537**, 59 (2014).

[60] M. Repisky, L. Konecny, M. Kadek, S. Komorovsky, O. L. Malkin, V. G. Malkin, and K. Ruud, J. Chem. Theory Comput. **11**, 980 (2015).

[61] M. Kadek, L. Konecny, B. Gao, M. Repisky, and K. Ruud, Phys. Chem. Chem. Phys. **17**, 22566 (2015).

[62] L. Konecny, M. Kadek, S. Komorovsky, O. L. Malkina, K. Ruud, and M. Repisky, J. Chem. Theory Comput. **12**, 5823 (2016).

[63]J. J. Goings, J. M. Kasper, F. Egidi, S. Sun, and X. Li, J. Chem. Phys. **145**, 104107 (2016).

[64]L. Rosenfeld, Z. Phys. **52**, 161 (1929).

[65]D. J. Tannor, *Introduction to Quantum Mechanics: A Time-Dependent Perspective* (University Science Books, Sausalito, 2007), p. 67.

[66]C. A. Ullrich, *Time-Dependent Density-Functional Theory: Concepts and Applications* (OUP, Oxford, 2011), pp. 59–72.

[67]R. Kosloff, J. Phys. Chem. **92**, 2087 (1988).

[68]A. Castro, M. A. L. Marques, and A. Rubio, J. Chem. Phys. **121**, 3425 (2004).

[69]X. Li, S. M. Smith, A. N. Markevitch, D. A. Romanov, R. J. Levis, and H. B. Schlegel, Phys. Chem. Chem. Phys. **7**, 233 (2005).

[70]C. Lubich, *From Quantum to Classical Molecular Dynamics: Reduced Models and Numerical Analysis* (European Mathematical Society, Zürich, 2008), pp. 63–104.

[71]D. Kidd, C. Covington, and K. Varga, Phys. Rev. E **96**, 063307 (2017).

[72]Y. Zhu and J. M. Herbert, J. Chem. Phys. **148**, 044117 (2018).

[73]A. Gómez Pueyo, M. A. Marques, A. Rubio, and A. Castro, J. Chem. Theory Comput. **14**, 3040 (2018).

[74]P. Bader, S. Blanes, and N. Kopylov, J. Chem. Phys. **148**, 244109 (2018).

[75]C. van Wüllen, J. Comput. Chem. **23**, 779 (2002).

[76]S. Komorovsky, M. Repisky, E. Malkin, T. B. Demissie, and K. Ruud, J. Chem. Theory Comput. **11**, 3729 (2015).

[77]B. A. Heß, C. M. Marian, U. Wahlgren, and O. Gropen, Chem. Phys. Lett. **251**, 365 (1996).

[78]D. Peng, W. Liu, Y. Xiao, and L. Cheng, J. Chem. Phys. **127**, 104106 (2007).

[79]J. Sikkema, L. Visscher, T. Saue, and M. Iliaš, J. Chem. Phys. **131**, 124116 (2009).

[80]D. Peng and M. Reiher, J. Chem. Phys. **136**, 244108 (2012).

[81]J. Liu and L. Cheng, J. Chem. Phys. **148**, 144108 (2018).

[82]B. Dunlap, J. Mol. Struct.: THEOCHEM **529**, 37 (2000).

[83]K. Eichkorn, O. Treutler, H. Öhm, M. Häser, and R. Ahlrichs, Chem. Phys. Lett. **240**, 283 (1995).

[84]L. Belpassi, F. Tarantelli, A. Sgamellotti, and H. M. Quiney, J. Chem. Phys. **124**, 124104 (2006).

[85]M. S. Kelley and T. Shiozaki, J. Chem. Phys. **138**, 204113 (2013).

[86]T. Saue, K. Fægri, T. Helgaker, and O. Gropen, Mol. Phys. **91**, 937 (1997).

[87]N. Rosch, Chem. Phys. **80**, 1 (1983).

[88]T. Shiozaki, Mol. Phys. **115**, 5 (2017).

[89]T. Saue and H. J. A. Jensen, J. Chem. Phys. **111**, 6211 (1999).

[90]G. te Velde, F. M. Bickelhaupt, E. J. Baerends, C. Fonseca Guerra, S. J. A. van Gisbergen, J. G. Snijders, and T. Ziegler, J. Comput. Chem. **22**, 931 (2001).

[91]E. J. Baerends, T. Ziegler *et al.*, ADF2017, SCM, Theoretical Chemistry, Vrije Universiteit, Amsterdam, The Netherlands, https://www.scm.com.

[92]E. van Lenthe, A. Ehlers, and E.-J. Baerends, J. Chem. Phys. **110**, 8943 (1999).

[93]J. P. Perdew, K. Burke, and M. Ernzerhof, Phys. Rev. Lett. **77**, 3865 (1996).

[94]J. P. Perdew, K. Burke, and M. Ernzerhof, Phys. Rev. Lett. **78**, 1396 (1997).

[95]J. C. Slater, Phys. Rev. **81**, 385 (1951).

[96]E. Van Lenthe and E. J. Baerends, J. Comput. Chem. **24**, 1142 (2003).

[97]ReSpect 5.0.1 (2018), relativistic spectroscopy DFT program of authors M. Repisky, S. Komorovsky, V. G. Malkin, O. L. Malkina, M. Kaupp, and K. Ruud, with contributions from R. Bast, R. Di Remigio, U. Ekstrom, M. Kadek, S. Knecht, L. Konecny, E. Malkin, and I. Malkin Ondik, see http://www.respectprogram.org.

[98]K. G. Dyall, Theor. Chem. Acc. **99**, 366 (1998).

[99]K. G. Dyall, Theor. Chem. Acc. **115**, 441 (2006).

[100]K. G. Dyall, Theor. Chem. Acc. **131**, 1172 (2012).

[101]R. A. Kendall, T. H. Dunning, Jr., and R. J. Harrison, J. Chem. Phys. **96**, 6796 (1992).

[102]D. E. Woon and T. H. Dunning, Jr., J. Chem. Phys. **98**, 1358 (1993).

[103]A. K. Wilson, D. E. Woon, K. A. Peterson, and T. H. Dunning, Jr., J. Chem. Phys. **110**, 7667 (1999).

[104]E. Malkin, M. Repisky, S. Komorovsky, P. Mach, O. L. Malkina, and V. G. Malkin, J. Chem. Phys. **134**, 044111 (2011).

[105]L. Visscher and K. G. Dyall, At. Data Nucl. Data Tables **67**, 207 (1997).

[106]E. Jones, T. Oliphant, and P. Peterson, SciPy: Open source scientific tools for Python, (2001), see http://www.scipy.org/.